Auditory-nerve first-spike latency and auditory absolute threshold: A computer model

Ray Meddis[a)]
Centre for the Neural Basis of Hearing at Essex, Department of Psychology, University of Essex, Colchester, CO4 3SQ, United Kingdom

(Received 30 June 2005; revised 25 October 2005; accepted 25 October 2005)

A computer model of the auditory periphery was used to address the question of what constitutes the physiological substrate of absolute auditory threshold. The model was first evaluated to show that it is consistent with experimental findings that auditory-nerve fiber spikes can be predicted to occur when the running integral of stimulus pressure reaches some critical value [P. Heil and H. Neubauer, J. Neurosci. **15**, 7404–7415 (2001)]. It was then modified to examine two ways in which the accumulation and clearance of receptor presynaptic calcium might explain this effect. Both methods gave results that matched the animal data. It was also shown how the rate of clearance of presynaptic calcium could be used to explain the origin of differences between low and high spontaneous-rate fiber types. When spiking activity is aggregated across a number of similar high spontaneous-rate fibers and used as the input to a model of a cochlear nucleus coincidence neuron, its response can be used to judge whether or not a stimulus is present. A simulated psychophysical experiment then demonstrated that this simple decision procedure can reproduce measurements of absolute auditory threshold for tones in quiet where the threshold is a joint function of both time and level. © *2006 Acoustical Society of America.* [DOI: 10.1121/1.2139628]

PACS number(s): 43.64.Bt, 43.64.Ld, 43.66.Ba, 43.66.Cb [BLM] Pages: 406–417

I. INTRODUCTION

The physiological basis of auditory absolute threshold is not known. Psychophysical thresholds are lower for longer stimuli and must therefore involve some kind of integration across time (see Eddins and Green, 1995 for a review). The physiological nature and anatomical location of this integrator is also unknown, and this is a major problem for computer models of the auditory system that seek to explain psychophysical phenomena in terms of a physiological substrate.

A number of studies in mammals (Clock *et al.*, 1998; Gersuni, 1965; Viemeister *et al.*, 1992) have used 2 interval, 2 alternative forced-choice (2I2AFC) paradigms to estimate absolute threshold on the basis of auditory-nerve (AN) fiber spike counts. These estimates show a similar trading relationship between stimulus level and duration to that found in behavioral measurements. Clock *et al.* (1993) used a similar paradigm but based threshold estimates on the spike counts of primary-like and chopper neurons in the ventral cochlear nucleus (CN) and showed a decline in threshold between stimulus durations of 8 and 128 ms. These animal studies show that the AN and CN responses are consistent with the phenomenon of temporal integration at absolute threshold. However, they do not identify the nature or location of the integrator. These experiments also carry the implication (but do not prove) that the temporal integration takes the form of spike counting at some anatomical location more central than the AN or CN.

However, Heil and Neubauer (2001) have presented evidence of a long-duration (>100 ms) example of temporal integration occurring at a very early stage in the auditory processing sequence, probably as early as the inner hair cell (IHC). Using single-fiber AN recordings, they showed that the latency to the first spike following stimulus onset is a function of both the amplitude and onset duration of the stimulus. For example, if two pure-tone stimuli have equal amplitudes but onset ramps of different duration, the stimulus with the shallower ramp will produce a later first spike. Heil and Neubauer showed that the best predictor of first-spike latency was the running integral of the stimulus pressure envelope. The first spike occurred when this integral reached a critical value, T_c (see Fig. 1). This critical value was consistent over time within a single fiber but varied meaningfully between fibers; for example, it was higher for low spontaneous rate (LSR) than for high spontaneous rate (HSR) fibers.

Heil and Neubauer (2003) went on to argue that the time constants of integration revealed by their observations were similar to those observed in the measurement of auditory thresholds. They make the radical argument that the temporal integrator is located *before* the AN. The computer modeling study below aims to demonstrate in physiological terms how temporal integration at this early stage could give rise to the time/duration trade-off observed in behavioral studies of absolute threshold.

Heil and Neubauer reasoned that the integrator must involve the accumulation of presynaptic calcium in the IHC. During acoustic stimulation, the receptor potential rises and calcium flows proportionately into the IHC in its presynaptic regions. It is this calcium that promotes the release of transmitter substance that initiates a postsynaptic action potential in the auditory-nerve fiber. This process constitutes a "leaky integrator" because the calcium is cleared from the presyn-

[a)]Electronic mail: rmeddis@essex.ac.uk

 © 2006 Acoustical Society of America

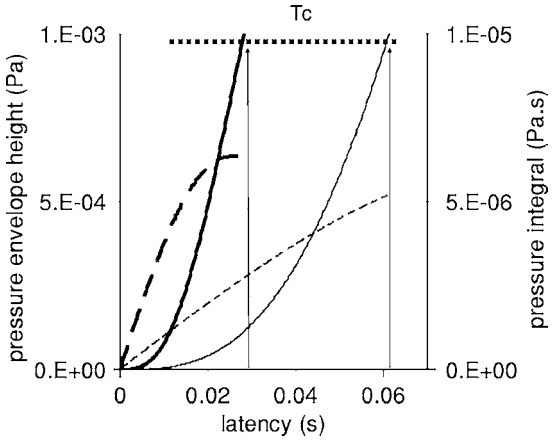

FIG. 1. General scheme of pressure integration paradigm. Dashed lines show two stimulus ramps (pressure: left ordinate). Continuous lines show the integral of stimulus pressure (pressure × time: right ordinate) for the two ramps. Predicted latency is the time, L, at which the integral of the pressure exceeds a critical threshold value, T_c.

aptic region almost (but not quite) as quickly as it arrives. They reasoned that the difference between LSR fibers and HSR fibers might be related to the rate at which the calcium builds up. In HSR fibers, it builds up quickly and this results in an early first spike. In LSR fibers the buildup of calcium is slower and the first spike is delayed.

It will be reported that this process was studied using an existing computer model of the auditory periphery (Sumner *et al.*, 2002, 2003a, 2003b, Holmes *et al.*, 2004, Meddis and O'Mard, 2005). The published model already incorporates a process where HSR fiber types were distinguished from LSR fiber types in terms of the rate of influx of calcium into the IHC. However, Heil and Neubauer also argue that it is not clear whether this faster accumulation of calcium in HSR fibers is the result of a higher rate of calcium influx into HSR synaptic regions or a slower rate of clearance. Both possibilities will be evaluated below and shown to be equally applicable. In the first "calcium influx" case, the published model was used. In the second "calcium clearance" case, the original model was used but different parameters were used to simulate the difference between fiber types.

It was then necessary to establish a direct connection between these processes and behavioral threshold. At first sight, this is straightforward. Near threshold, the first-spike latency will determine whether or not the stimulus provokes a detection decision. If the duration of the stimulus is shorter than the expected first-spike latency, then no spike will occur and the stimulus will be undetected. If, however, the same stimulus is presented at a greater intensity, the first spike will occur at an earlier time which is more likely to be before the end of the stimulus. In the absence of spontaneous activity, the detection of the stimulus could depend on a single spike occurring in a single fiber. Unfortunately, the fibers with the lowest thresholds are also the fibers with the highest rate of spontaneous activity (e.g., Liberman and Kiang, 1978; Winter *et al.*, 1990). This creates the problem of how the auditory system distinguishes between spontaneous spikes and stimulus-driven spikes.

In this computer modeling study, it is proposed that the problem can be solved by combining spikes across a group of similar AN fibers. In the proposed model, a number of model HSR AN fibers supply input to a model CN neuron that is configured as a "coincidence detector," one that responds only when a number of input spikes occur almost simultaneously. In quiet, the HSR fibers spike at random with respect to one another and do not trigger a response in the CN unit. When the AN fiber activity is driven by an acoustic stimulus, the spike activity is correlated. In particular, the first spikes will occur at similar times because similar fibers have similar expected first-spike latencies. As a consequence, spontaneous spikes will not cause a response in the CN unit, but stimulus-driven spikes will do so and the stimulus will be detected. It will be shown that this model displays the expected trade-off between stimulus level and duration when tested in a psychophysical 2I2AFC paradigm.

Only one other relevant modeling study has been published (Krishna, 2002). He used a more schematic computer model successfully to simulate first-spike latency data. His model was successful because it includes an explicit "integration module" with a critical threshold function. Although the model is physiologically inspired, this integration module was not associated with any specific physiological function except that the author explicitly *ruled out* the possibility that it could be calcium dynamics. This rejection was based on the grounds that the time constants of calcium dynamics were too short. The following study will show that this widely held objection is not well founded. Indeed, the rapid dynamics of presynaptic calcium are ideally suited to the long time scales of the first-spike latency effect.

II. COMPUTER MODEL

The input to the computer model of the auditory periphery is an arbitrary acoustic stimulus. Its output is a stream of spiking events in one or more parallel AN fibers all innervating the same location on the cochlear partition. The complete peripheral model consists of a cascade of six stages estimating: (1) stapes velocity; (2) BM velocity; (3) IHC receptor potential; (4) IHC presynaptic calcium currents; (5) transmitter release events at the IHC-AN synapse; and (6) AN spiking response including refractory effects. The output of the peripheral model is used as input to a second model of a single cochlear nucleus chopper neuron. Throughout this study all AN fibers have a best frequency of 4 kHz and all stimuli are 4-kHz tones. The basilar-membrane response in this implementation of the model is linear up to 40 dB SPL. As a consequence, BM nonlinearity does not feature in the evaluation of absolute threshold where most stimuli are presented well below this level.

A complete description of the model equations and parameters is given in the Appendix. Except where specified, all equations and parameters are exactly as specified in the most recent previously published evaluations of the component modules. The model was implemented using routines from a library of C-code modules in the Development System for Auditory Modeling (DSAM) which is published by

the University of Essex, UK. The full model of the auditory periphery was implemented as a program sequence using the AUDITORY MODELLING SYSTEM (AMS) application.[1] The MATLAB programming language was used to create the sequence of stimuli, to initiate a model run, and to collect, analyze, and display the results. The model was evaluated at a sampling rate of 100 kHz.

A. Presynaptic calcium

Two models of calcium dynamics are evaluated below. The first model (calcium influx) identifies the difference between AN fiber types in terms of different rates of influx of calcium into the cell and assumes, for example, that LSR fibers have the lowest rate of calcium influx for a given receptor potential. The second model (calcium clearance) assumes a fixed rate of influx for all fiber types, but defines the differences between fibers in terms of the rate at which calcium is cleared from the presynaptic site. LSR fibers, for example, have the fastest rate of clearance of presynaptic calcium.

1. Calcium influx model

Calcium concentration, $[Ca^{2+}](t)$, is modeled as a first-order low-pass filtered function of the trans-membrane calcium current, $I_{Ca}(t)$

$$\frac{d[Ca^{2+}](t)}{dt} = I_{Ca}(t) - [Ca^{2+}](t)/\tau_{Ca}, \tag{1}$$

where τ_{Ca} is the time constant of calcium clearance and

$$I_{Ca}(t) = G_{Ca}^{max} m_{I_{Ca}}^3(t)(V(t) - E_{Ca}), \tag{2}$$

where $V(t)$ is the receptor potential, E_{Ca} is the reversal potential for calcium, and G_{Ca}^{max} is the maximum calcium conductance in the vicinity of the synapse, $m_{I_{Ca}}(t)$ is the fraction of calcium channels that are open and is a function of the receptor potential (see the Appendix for the determination of $m_{I_{Ca}}$). The probability that an available transmitter vesicle will be released into the synaptic cleft is proportional to the cube of the $[Ca^{2+}]$ concentration

$$k(t) = \max(([Ca^{2+}]^3(t) - [Ca^{2+}]_{thr}^3)z, 0), \tag{3}$$

where z is a scalar and $[Ca^{2+}]_{thr}^3$ is a threshold parameter. Both G_{Ca}^{max} and $[Ca^{2+}]_{thr}^3$ are changed when modeling the difference between LSR and HSR fibers. This model is unchanged from its previously published form.

2. Calcium clearance hypothesis

Evaluation 2 investigates Heil and Neubauer's proposal that differences between AN fibers might alternatively be explained in terms of differences in the rate of calcium clearance. To evaluate this proposal the same model was used except that the time constant of calcium clearance, τ_{Ca}, was changed when modeling the difference between fibers, while G_{Ca}^{max} was held constant and $[Ca^{2+}]_{thr}^3$ was set to zero. This allows us to simplify Eq. (3) so that the relationship between calcium levels and transmitter release is more transparent.

$$k(t) = z\,Ca^3(t). \tag{4}$$

In this version, only τ_{Ca} ic changed when modeling the difference between LSR and HSR fiber types.

III. EVALUATION 1: CALCIUM INFLUX MODEL

Heil and Neubauer (2001, 2003) measured the "latency to first spike" of single AN fibers in cat in response to pure tones. Both the level of the tones and the steepness of the onset ramp were varied. The following demonstration replicates their experimental procedure in detail using the computer model of the guinea pig periphery. Model parameters were unchanged from Sumner *et al.*, 2002, 2003a and 2003b, but incorporated small changes described in Meddis and O'Mard (2005). All parameters are given in the Appendix and the rate/level functions for this model are shown in Fig. 3(A) (below).

Pure-tone stimuli at BF (4 kHz) of 200-ms duration were shaped with cosine-squared rise and fall functions with seven different rise times equally spaced on a log scale between 1.7 and 170 ms. They were presented at levels that varied between 0 and 90 dB SPL in 10-dB steps. Each stimulus was presented 20 times and the mean latency to first spike was measured for each presentation. Latencies were measured between the beginning of the stimulus onset ramp and the first spike that occurred after that time. If no spike occurred before the end of any stimulus on any of the 20 trials, the mean latency for that combination of level and ramp duration was treated as indeterminate. Each trial began with a 50-ms period of silence which was used to assess the spontaneous firing rate. Figure 2 (top row) shows model first-spike latencies measured as a function of both level and ramp duration.

Heil and Neubauer showed that the mean latencies (L) for the animal data could be predicted, L_{pred}, by the sum of two quantities, L_{min} and L_c, where L_{min} is a minimum latency common to all measurements for that fiber and L_c is the delay before the integral of the pressure envelope reaches a critical threshold value T_c (measured in Pa s). These two free parameters, L_{min} and T_c, were estimated by finding the least-squares best fit between the logarithms of the predicted and actual latencies (see Heil and Neubauer, 2001, for a full account of the relevant procedures and justification). Measured latencies were used in the calculations only if these were shorter than half the average interval between spikes during spontaneous activity. Figure 2 (bottom row) plots the actual latencies of the present model against the latencies predicted by Heil and Neubauer's formula as a function of tone level and ramp duration.

HSR, MSR, and LSR model fibers all show the expected effect and the plots are virtually identical with those given by Heil and Neubauer [2001, Figs. 2(B), 5(A)–(D), 6(A) and (C)]. The small deviations from the predicted line (diagonal) for short and long predicted latencies are also a characteristic of the animal data [Heil and Neubauer, 2001, Figs. 6(A) and (C)] and are not a shortcoming of the model. These deviations reflect the fact that the calcium integration system is "leaky" and, as a consequence, is not a perfect integrator of stimulus pressure. Heil and Neubauer [2001, Fig. 8(D)] ob-

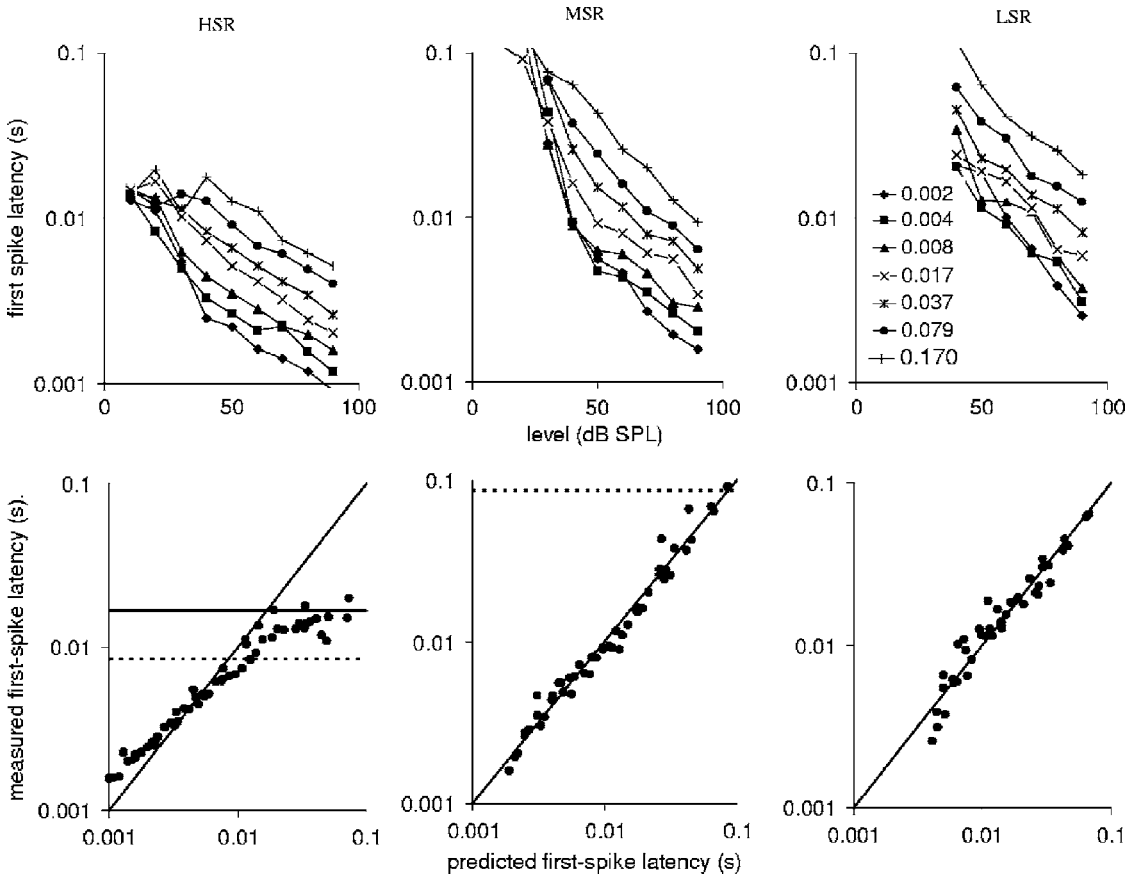

FIG. 2. Model AN first-spike latencies using the calcium influx model for HSR, MSR, and LSR fiber types. Top row: first-spike latencies as a function of tone level (x axis) and onset ramp duration (see the legend). Bottom row: first-spike latencies as a function of predicted latencies using the prediction function $L_{\text{pred}}=L_{\text{min}}+L_c$ (see the text). The horizontal continuous line represents the expected latency during spontaneous activity (1/spontaneous rate). Horizontal dotted lines indicate the cutoff criterion for omitting data from the best-fit analysis for the prediction function. The best-fit values for L_{min} are 1, 2, and 3 ms for HSR, MSR, and LSR fibers, respectively. The corresponding values for T_c are 5.3E-6, 1.7E-5, and 1E-4 Pa s.

tained critical threshold integrals (T_c) in the region 1E −7 to 1E−4 Pa s. The values shown in Fig. 2 are comfortably within that region. They also found that T_c was greater for LSR than HSR fibers. This was also true of the model data.

IV. EVALUATION 2: CALCIUM CLEARANCE MODEL

Heil and Neubauer speculated that the rate of clearance of calcium from the presynaptic region might also be a critical parameter determining first-spike latency, and that the variation in spontaneous rate across nerve fibers might be explained in terms of differences in the rate of calcium clearance. In the calcium influx model, the calcium clearance time constant (τ_{Ca}) is fixed while the rate of calcium influx per unit of time varies across fiber types. To test the new hypothesis (that influx is fixed while τ_{Ca} varies across fiber types), the model was run again varying τ_{Ca} while holding other parameters constant.

Figure 3 shows the rate-level function for both the original calcium influx model and the calcium clearance version of the model. The results show that both models give a useful account of the differences between fiber types similar to

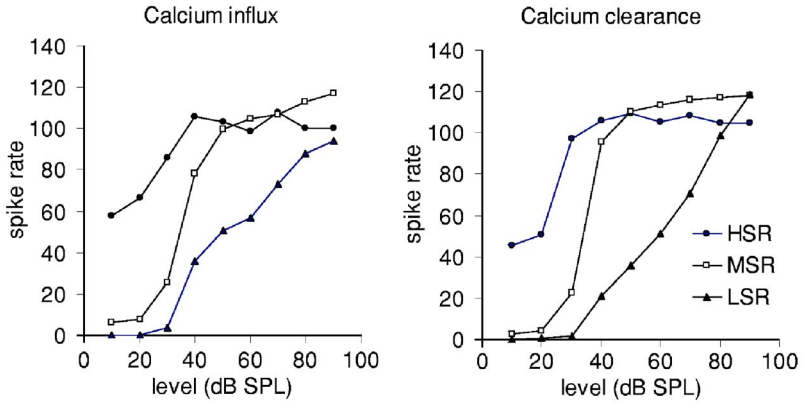

FIG. 3. Rate-level functions for the original and modified calcium influx models. Rate is based on all spikes during presentation of a 200-ms pure tone presented at CF (4 kHz). Tones had a 17-ms cosine-squared onset ramp. In the calcium clearance model, τ_{Ca} values were 0.35, 0.15, and 0.075 ms for HSR, MSR, and LSR fibers, respectively.

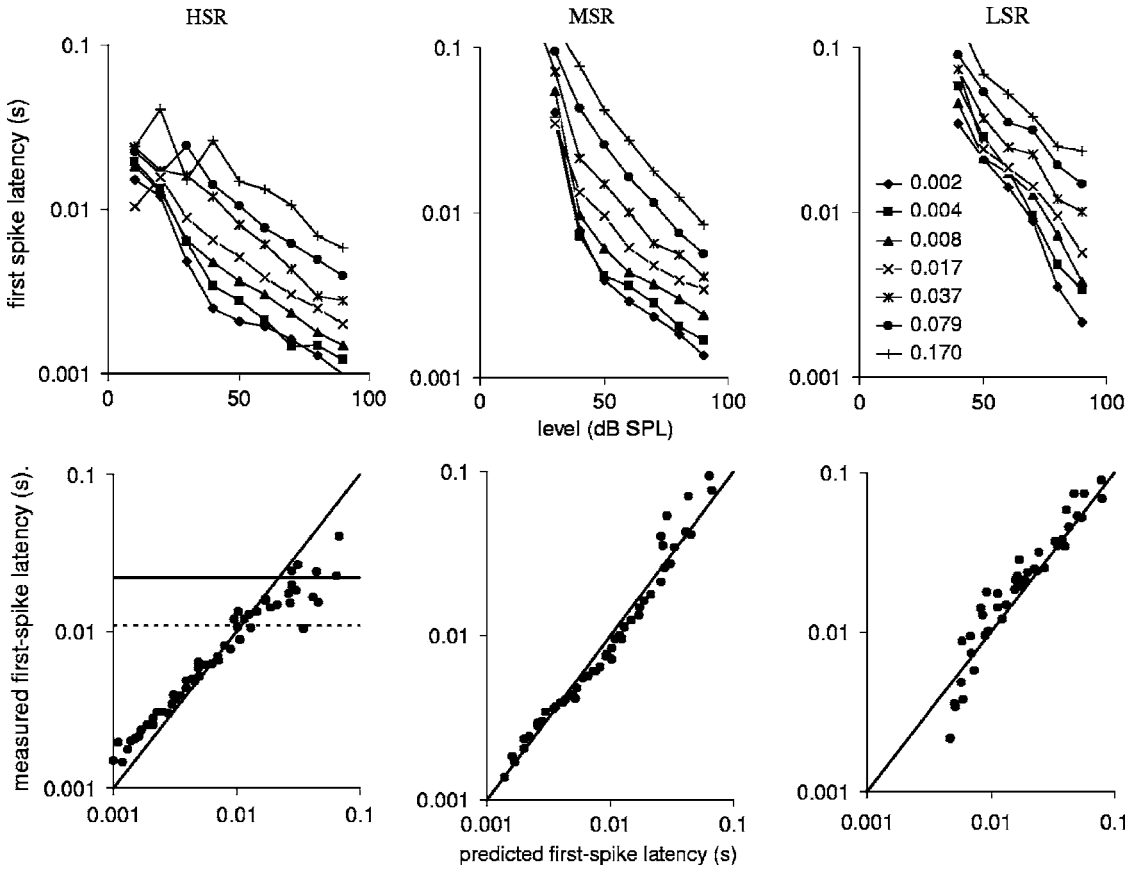

FIG. 4. Model first-spike latency using the calcium clearance model for HSR, MSR, and LSR fiber types. (See Fig. 2 for explanation). The best-fit values for $L_{\min}$ are 1, 1, and 6 ms for HSR, MSR, and LSR fibers, respectively. The corresponding values for T_c are 5.3*E*-6, 1.7*E*-5, and 1*E*-4 Pa s.

those observed in laboratory studies. HSR fibers have higher spontaneous rates, a lower rate threshold, and a lower saturation threshold than LSR fibers. The differences in the shape of the rate-level functions are similar to the differences observed between LSR and HSR fibers in mammalian physiological studies (Liberman and Kiang, 1978; Winter *et al.*, 1990).

First-spike latency data for the same three fiber types are shown in Fig. 4. They show the same pattern as the data in Fig. 2. Once again, the critical pressure integral required to fit the response of the modified model lies within the range observed by Heil and Neubauer and the critical pressure integral, T_C, increases across the HSR-LSR spectrum. In conclusion, both the calcium-influx model and clearance models are able to simulate both the first-spike latency effect and the differences between fiber types. They are, therefore, both candidate explanations in terms of presynaptic calcium dynamics.

The central difference between the two models is, of course, an empirical issue. The question as to whether the low spontaneous firing rate of LSR fibers is caused by different rates of clearance or different rates of calcium influx is more properly decided by further laboratory observation. In evaluations 3 and 4 below, both models were tested and gave approximately the same results. The illustrations below use only the calcium-clearance model for the only reason that it is slightly simpler. By dispensing with the calcium threshold parameter, $[Ca^{2+}]^3_{thr}$, it requires only one parameter to distinguish HSR and LSR fibers while the calcium influx version uses two [see Sumner *et al.* (2002, Fig. 5)].

For both models, it should also be noted that the critical threshold integral, T_c, as estimated from the first-spike latencies, is *not* a parameter of the model but an emergent property. When the presynaptic calcium level rises, the probability of release of a transmitter vesicle rises as a function of the third power of the calcium level. As a consequence, the probability of a release event increases very rapidly. However, there is no "trigger" calcium threshold, *per se*, in the model, only the *appearance* of one.

V. EVALUATION 3: COINCIDENCE DETECTION

The first-spike latency data provide evidence that temporal integration of a kind is taking place at an early stage in the auditory system. The integration takes place over relatively long time periods (more than 100 ms). This suggests that the first-spike latency might be related to the temporal integration observed in psychophysical studies. One possibility is that the nervous system fails to detect low-intensity, short sounds because the time taken to accumulate enough presynaptic calcium to initiate a spike is greater than the duration of the signal. If the signal is too weak or too short, no spike is initiated before the end of the signal and no detection occurs.

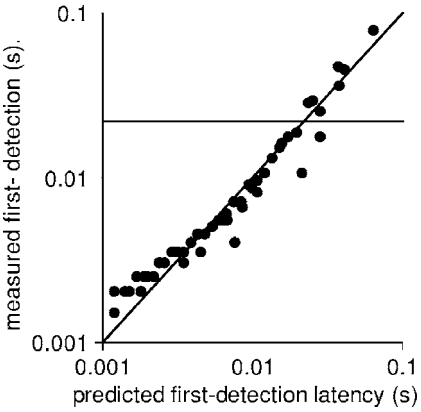

FIG. 5. First-spike latency of a model *CN coincidence neuron* plotted against predicted first-spike latency. The neuron receives input from 20 model HSR fibers. The horizontal continuous line is the "expected latency" (1/spontaneous rate) of the AN fibers used as input.

The next stage of the model addresses the problem of how to distinguish spontaneous AN spikes from spikes that are stimulus driven using the principle outlined in the Introduction. The model is extended so that 20 HSR AN model fibers are used as input into a coincidence-detector neuron. This consists of two stages; a low-pass filter to simulate dendritic smoothing followed by a simple computer model of the neuron soma (MacGregor, 1987) described in the Appendix and elsewhere (Hewitt and Meddis, 1993; Wiegrebe and Meddis, 2004). This unit has a spontaneous rate of 1.5 spikes/s. When acoustically stimulated, it responds with a sustained chopper firing pattern. The dendritic filter has a low-pass cutoff of 200 Hz which equates to a time constant of approximately 0.7 ms. As a result, the CN unit responds only when the input fibers generate spikes very close together in time. This is roughly equivalent to a previous implementation of the same principle (Meddis and O'Mard, 2005) where the inputs were simply aggregated into 0.5-ms bins and a minimum count criterion applied.

In this evaluation, the protocol of stimulus presentation is exactly the same as that used in evaluations 1 and 2 except that latency is based on the first spike produced by the CN neuron. The results are shown in Fig. 5 where the diagonal line shows the predicted latency estimated using the same procedure used earlier with AN fibers. The coincidence latencies are a good fit to the prediction, and the correspondence between predicted and actual latencies shows a greatly extended temporal range. For HSR AN fibers the relationship between first-spike latency and pressure integral is valid only up to approximately 10 ms (see Fig. 4). This is because the spontaneous activity of the fiber introduces an upper limit to the length of intervals occurring between successive spikes. When the coincidence criterion is used, this limitation is removed because the coincidence neuron does not respond to spontaneous AN spikes. The figure shows that the relationship remains valid up to at least 100 ms.

VI. EVALUATION 4: CN AND PSYCHOPHYSICAL THRESHOLDS

The results obtained in evaluation 3 suggest that the coincidence detection model might be capable of temporal integration over the longer time scales that characterize *psychophysical* paradigms. A low-intensity stimulus will produce a coincidence event with a long latency. If that stimulus is short, the coincidence event will not occur before its termination. As a result, the length of the signal will be critical in determining whether it is detected at all. To evaluate this possibility, the absolute threshold of the model was measured as a function of stimulus duration. The procedure was based as closely as possible on a 2I2AFC psychophysical experiment described by Florentine *et al.* (1988).

In the same evaluation, the model response is compared to the results of a corresponding animal study (Clock *et al.*, 1993) where CN unit responses were recorded in a 2I2AFC paradigm. They also drew attention to a statistical complication associated with the method of counting CN unit spikes. They began by assuming that the decision was made by an "ideal observer" with complete knowledge of the time of the onset and offset of the stimulus so that probe-spike counts were restricted to the time that the probe was on ("probe-count" measure). However, it cannot always be assumed that the decision process always knows exactly when a stimulus will occur or how long it will last. For example, in the experiment with human listeners, the stimuli (irrespective of their length) were presented during a 550-ms inspection window, and listeners would need to base their decision on spike activity throughout the whole period ("window-count" measure). The statistical nature of the decision is, in principle, different for the two measures. Clock *et al.* studied both approaches and both will be considered below.

Absolute thresholds were measured using a 2I2AFC paradigm following as closely as possible the protocol of Florentine *et al.* (1988). On each trial, two independent 550 -ms observation intervals were used; one silent interval and one containing a probe tone presented central to the observation window. The model's task was to use the output of the coincidence detection neuron to choose which interval contained the stimulus. Threshold measurements were made using a two-down, one-up adaptive procedure which converges on the signal level yielding 70.7%-correct responses (Levitt, 1971). The probe level started at 50 dB SPL and was reduced by steps of 5 dB until the first reversal, after which the step size was reduced to 2 dB. A run was terminated after five reversals and thresholds were calculated using the average level of the last two reversals. Stimuli were pure tones presented at CF (4 kHz) with rise times of 1 ms. Separate threshold estimates were made for signal durations of 2, 4, 8, 16, 32, 64, 128, 256, and 512 ms.

For each of the two observation intervals, the model made an independent decision as to whether a stimulus was or was not present. A "yes" decision was made if the neuron generated *at least one spike* during the counting period. Separate decisions were made for the stimulus and control condition. If only one interval generated a yes response, that interval was chosen. If the same decision was made for both intervals, either yes for both or "no" for both, the model chose one of the two alternatives at random. In the example below, the spontaneous rate of the CN neuron was very low (<2 spikes/s). Near threshold, the spike count was typically zero or 1. A special provision was made for occasions arising

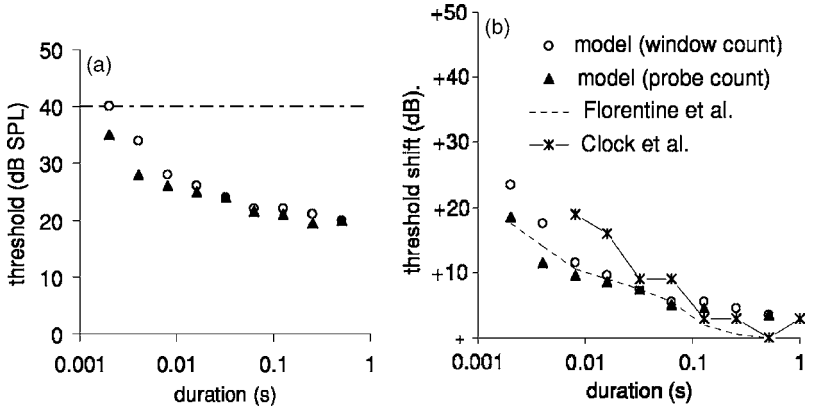

FIG. 6. (a) Absolute threshold of a model cochlear nucleus coincidence neuron as a function of signal duration. Thresholds are based on total spike counts in the 500-ms observation window (open circles) or exclusively when the probe was playing (filled triangles). Each threshold is the mean of 20 trials. Stimuli are CF (4-kHz) tones. The horizontal dotted line indicates the level at which basilar-membrane compression begins in the basilar-membrane stage of the model. (b) Threshold shift representation of the same data. Also shown are human data (Florentine *et al.*, 1988; dashed line) and animal CN unit thresholds (Clock *et al.*, 1993; asterisks). The human data are adjusted to give 0-dB shift at the longest duration. The model data are shifted so that the middle durations approximately match the human data. This emphasizes the slope differences at the longest and shortest durations.

at the beginning of the trial when the stimulus was well above threshold and the spike count for the stimulus-present condition was very large with respect to the stimulus-absent condition. In the event of a yes/yes outcome when the discrepancy in the counts was very large, the decision was given in favor of the window yielding the larger count in order to move the stimulus level more quickly towards the threshold region. Once in the threshold region, this principle was no longer needed.

The model was exactly the same as that described in evaluation 3. Figure 6(a) shows absolute threshold as a function of signal duration based on both methods of calculating spike counts (see above). Threshold decreases monotonically between 2 and 512 ms. All but one of the thresholds are below the compression threshold for the basilar-membrane simulation (horizontal dotted line). Nonlinearity of response was, therefore, unlikely to contribute to the determination of the threshold. The probe-count and window-count datasets are similar except at very short durations when the precise knowledge of the time and duration of the stimulus produces a small but consistent reduction of threshold.

Figure 6(b) compares the same data with the psychophysical thresholds of Florentine *et al.* (1988, Fig. 1; mean of five listeners) and the physiological measurements of Clock *et al.* (1993) based on single unit measurements in the CN. The model data have been adjusted slightly so that they are close to the human data in the mid-duration range. The model data fit the human data reasonably well up to 64 ms. Both the model and the human data have roughly level functions at very long durations. However, the leveling begins earlier for the model data. It is difficult to know how significant these differences are. The reduction in threshold between 100 and 500 ms is very small for the psychophysical data nine other studies reviewed by Florentine *et al.* (1988) are inconsistent in this region.

Clock *et al.* speculated that the spike counts based on the probe period alone might be subject to a statistical artifact because the observation window was changing in size across different signal conditions. They measured the mean (M) and standard deviation (SD) statistics of spike counts and found that the ratio SD/M decreased with duration up to 128 ms and then leveled out at long durations. This means that an "ideal observer" who takes advantage of knowledge of the time of occurrence of the probe should show an improved ability to distinguish between signal and noise up to 128 ms. This is consistent with the model response where the probe count showed lower thresholds for the shortest stimuli. The best fit to human data at short durations is obtained using the probe-count method and is, therefore, consistent with the idea that the human observer is taking advantage of knowledge of the expected time and duration of delivery of the probe during the observation window.

VII. DISCUSSION

Evaluation 1 showed that a previously published model of IHC synapse function could simulate the basic first-spike latency findings of Heil and Neubauer (2001). The model first-spike latency could be predicted on the basis of the integral of the stimulus pressure envelope between the onset of the tone stimulus and the time of the first spike. The pressure integral (T_c) at which the first spike typically occurred was lower for HSR than LSR fibers. This is also in agreement with the animal data. The model latencies can be attributed to the accumulation of presynaptic calcium during tone presentation. The effect was shown to operate at least up to tone durations of 200 ms.

Evaluation 2 modified the model so that fiber type was controlled using the rate of clearance of calcium from the presynaptic region. This model generated realistic rate-level functions for the different fiber types and was also able to simulate the first-spike latency data. In terms of performance, there was little to distinguish the two models. However, the modified model gave a simpler account of the IHC calcium dynamics and dispensed with the use of a specific threshold parameter. As a consequence, it is easier to see that the threshold differences between the fiber types are emergent properties rather than fixed properties of the model. In gen-

eral terms, the modeling work supports the conjecture of Heil and Neubauer that first-spike latency is determined by the accumulation of presynaptic calcium, but it does not help decide whether these differences are caused by different rates of calcium influx or clearance. It does show, however, that both possibilities are worthy of further investigation.

Evaluation 3 linked first-spike latency with absolute perceptual threshold by extending the model to include a CN coincidence neuron whose input was 20 HSR fibers. The neuron was tuned to be all but unresponsive to uncorrelated spontaneous activity but responsive to correlated stimulus-driven activity. CN latencies also showed a strong relationship to integrated pressure. However, this relationship remained valid over longer stimulus durations in the CN model than with the AN HSR fiber model. A relationship to integrated pressure was visible up to 100 ms in this test.

Evaluation 4 explored a possible link between AN first-spike latency and absolute perceptual threshold by simulating a psychophysical experiment (Florentine *et al.*, 1988) but substituting the model CN unit for the human listener. The model data were similar in number of respects to the human data. While the meaning of the correspondence can easily be overstated, it is clear that a coincidence detecting neuron receiving input from similar HSR fibers could show temporal integration up to 500 ms. The slope of the threshold-duration function is, however, less steep than the psychophysical data after 64 ms. The modeling result is similar to the measurements of Clock *et al.* (1993) in the CN.

This evaluation also addresses the more general issue of detecting isolated stimuli where the system has little prior knowledge of the stimulus timing. In a probe-count (ideal observer) condition, it was assumed that the system knew exactly when the stimulus will occur and how long it would be. In contrast, a window-count method assumed only that a stimulus of unknown duration would occur within a period of time that might be considerably longer than the stimulus. The probe-count approach produced lower thresholds for shorter stimuli than the window-count method but both showed a similar trading relationship between duration and level.

Until recently, it has been a common view that temporal integration must take place relatively late in the auditory processing sequence because the long duration of the integration period contrasts with the short time constants typically found in peripheral physiological processes. However, this is based on a misunderstanding; "leaky integrator" systems with short time constants are capable of integrating over long time periods if the input rate is rising and the time constant of clearance is fast.

A possible counterexample to the hypothesis modeled here is the finding of Gerken (1979) that the behavioral threshold in cat for brief electrical pulses delivered to electrodes in the CN of a cat decreased by 7.6 dB per tenfold (1.5 dB per octave) increase in the number of pulses. If this involves the same mechanism as psychophysical auditory temporal integration, then it would firmly locate the integration mechanism *after* the IHC/AN synapse, and the relationship between first-spike latency and integrated pressure could be seen as irrelevant. Unfortunately, the pulse data are open to a range of interpretations. One is that each threshold level pulse (taken as a separate entity) is associated with a small probability of eliciting a detection. As the number of pulses is increased, the probability that *at least one* pulse will be detected will increase proportionately. Accordingly, any interpretation of these data in terms of temporal integration should be treated with caution.

In this study, a sustained chopper unit was used as the decision neuron in the cochlear nucleus. Clock's results show that both primary-like and chopper units show the time-duration trade-off, and either could have been chosen for this project. The chopper unit also had the convenience of a low spontaneous rate (1.5 sp/s), which made it easier to illustrate the application of the coincidence principle. Nothing in this study rules out other possibilities.

Of course, the presence of any spontaneous activity in the decision unit will render the detection process less reliable. In principle, at least, additional decision reliability can be achieved by repeating the coincidence-detection process at a higher level, such as the inferior colliculus, so that the higher unit is insensitive to spontaneous activity in the CN. This may be part of the explanation as to why both the animal CN data and the model CN data did not show the expected decline in threshold beyond stimulus durations of 64 ms. The small amount of spontaneous activity would be expected to produce some random spike events during these longer stimuli and to raise thresholds proportionately.

However, the primary purpose of this study is not to identify the specific circuits involved but to show that the psychophysical data on thresholds for tones in silence are consistent with the idea that some temporal integration takes place in the IHC rather than later in the processing chain. In this respect, the current modeling exercise using only one CN neuron is primarily a practical demonstration that the temporal integration underlying thresholds in quiet might be taking place as early as the IHC. Neuronal processes subsequent to the AN are used in the model but theirs is a *decision function*. In the model at least, the temporal integration is complete before the AN.

The term "temporal integration" is used in psychophysics with reference to a wide range of suprathreshold phenomena (such as gap detection, loudness, and sensitivity to amplitude modulation) and also to the numerous theories that have been proposed to explain them (Eddins and Green, 1995). This model study concerns itself exclusively with the detection of pure tones in silence, and it is not suggested here that the calcium dynamics of the IHC can be used to explain the full range of phenomena in this class.

Empirical methods will eventually decide the question of what mechanisms underpin first-spike latency and psychophysical temporal integration at absolute threshold. However, the question of how we link the physiological substrate to absolute auditory threshold is a conceptual matter and well suited to exploration by modeling methods. The conventional view that equates the rate threshold of single AN fibers with behavioral threshold is clearly inadequate because threshold also depends on stimulus duration. The problem of stimulus detection near absolute threshold is further complicated by the presence of spontaneous activity in the nerve fiber. The

model evaluated here presents one solution to this problem by suggesting that the relevant units in the cochlear nucleus respond only when multiple AN fibers fire in synchrony. In this respect, it is convenient for the model that the temporal integration component has already taken place in the IHC/AN synapse. As a consequence, the level at which sound induces a response in at least one CN unit is a function of both time and level.

ACKNOWLEDGMENTS

This manuscript and the modeling has benefited substantially from the challenging and insightful comments of Brian Moore, Peter Heil, and Heinrich Neubauer on a much earlier version of this manuscript. Chris Sumner and Enrique Lopez-Poveda also contributed useful comments on a later manuscript. Lowel O'Mard contributed valuable computational support throughout.

APPENDIX: COMPUTATIONAL DETAILS

1. Middle-ear filtering

A cascade of two linear bandpass Butterworth filters was used to model the response of the guinea pig middle ear. The first filter is second order with an upper cutoff of 25 kHz and a lower cutoff of 4 kHz. The second filter is third order with upper- and lower-cutoffs of 30 and 0.7 kHz. Both have unit gain in the passband. The filter output is transformed into stapes velocity by applying a scalar of $1.4E{-}4$ m s^{-1} Pa^{-1}.

2. Mechanical filtering: DRNL filter

The filtering of the BM is modeled with a "dual-resonance-nonlinear" (DRNL) filter architecture that has been described and evaluated more fully elsewhere (Meddis *et al.*, 2001; Lopez-Poveda and Meddis, 2001; Sumner *et al.*, 2003b). The input is stapes velocity, $x(t)$. The DRNL filter consists of two parallel pathways, one linear and the other nonlinear, whose outputs are summed to produce an output, $v(t)$ representing the velocity of the cochlear partition in m s^{-1}.

The *nonlinear* pathway consists of the following cascaded sequence: (1) three identical first-order gammatone filters; (2) a compression function; (3) three more identical gammatone filters, and (4) four first-order Butterworth low-pass filters. The compression in the nonlinear pathway is described by

$$v_t = \mathrm{SIGN}(x_t) \times \mathrm{MIN}(a|x_t|, b|x_t|^{\upsilon}), \tag{A1}$$

where a and b are parameters specific to a particular BM location (see Table I). The compression exponent, υ, was 0.1. The *linear* pathway consists of the following cascaded sequence: (1) a gain function; (2) a cascade of three identical gammatone filters; (3) a cascade of four Butterworth low-pass filters. For both pathways the cutoff frequency of the low-pass filters was set to the CF of the corresponding gammatone filters.

TABLE I. Coefficients for computing parameters of the guinea pig DRNL filters as a function of CF_{nl}. Source: Sumner *et al.* (2003b).

$\log(\text{parameter}) = p_0 + m\log(CF_{nl})$	p_0	M
Bandwidth of nonlinear path, BW_{nl} (Hz).	0.8	0.58
Compression parameter, a	1.87	0.45
Compression parameter, b	−5.65	0.875
Center frequency of linear path, CF_{lin} (Hz).	0.339	0.895
Bandwidth of linear path, BW_{lin} (Hz).	1.3	0.53
Linear path gain, G_{lin}.	5.68	−0.97

The CF of the nonlinear path gammatone filters (CF_{nl}) is set to the desired CF of the filter as a whole. The other parameters of the system are set relative to CF_{nl} using the formula

$$\log(\text{parameter}) = p_0 + m\log(CF_{nl}). \tag{A2}$$

Table I shows the parameters p_0 and m used to compute the parameters a, b, the bandwidths of the component gammatone filters in linear (BW_{lin}) and nonlinear (BW_{nl}) pathways, the gain of the linear filter (G_{lin}), and the center frequency of the linear filter (CF_{lin}).

3. IHC receptor potential

The displacement of the IHC cilia, $u(t)$, as a function of BM velocity, $v(t)$, is given by

$$\tau_c \frac{du(t)}{dt} + u(t) = \tau_c C_{\mathrm{cilia}} v(t), \tag{A3}$$

where C_{cilia} is a gain factor and τ_c is a time constant. The cilia displacement determines the apical conductance $G(u)$. The total apical conductance is given by

$$G(u) = G_{\mathrm{cilia}}^{\max}\left[1 + \exp\left(-\frac{u(t)-u_0}{s_0}\right) \times \left[1 + \exp\left(-\frac{u(t)-u_1}{s_1}\right)\right]\right]^{-1} + G_a, \tag{A4}$$

where $G_{\mathrm{cilia}}^{\max}$ is the transduction conductance with all channels open, and G_a is the passive conductance in the apical membrane. s_0, u_0, s_1, and u_1 are constants determining the exact shape of the nonlinearity. G_a is computed as

$$Ga = G0 - G_{\mathrm{cilia}}^{\max}\left[1 + \exp\left(\frac{u_0}{s_0}\right)\left[1 + \exp\left(\frac{u_1}{s_1}\right)\right]\right]^{-1}, \tag{A5}$$

where $G0$ is the resting conductance. See Table II.

The membrane potential of the cell body is modeled with a passive electrical circuit analog

$$C_m \frac{dV(t)}{dt} + G(u)(V(t) - E_t) + G_k(V(t) - E_k') = 0, \tag{A6}$$

where $V(t)$ is the intracellular IHC potential; C_m is the cell capacitance; G_k is the voltage-invariant basolateral membrane conductance; E_t is the endocochlear potential; and $E_k' = E_k + E_t R_p/(R_t + R_p)$ is the reversal potential of the basal current E_k corrected for the resistance (R_t, R_p) of the supporting cells.

TABLE II. IHC receptor potential. Source: Sumner *et al.* (2002, Table I). Note that *s*1 was previously given incorrectly as $5E-7$.

Et, endocochlear potential (V)	$100E-3$
Ek, potassium reversal potential (V)	$-70.45E-3$
*G*0, resting conductance (S)	$1.974E-9$
Gk, potassium conductance (S)	$18E-9$
$Rp/(Rt+Rp)$, correction factor (Ω)	$40E-3$
$G_{\text{cilia}}^{\max}$, max. mechanical conductance (S)	$8E-9$
s_0, displacement sensitivity (m^{-1})	$85E-9$
u_0, displacement offset (m)	$7E-9$
s_1, displacement sensitivity (m^{-1})	$5E-9$
u_1, displacement offset (m)	$7E-9$
C_m, total capacitance (F)	$6E-12$
τ_c cilia/BM time constant (s)	$2.13E-3$
C_{cilia}, cilia/BM coupling gain (dB)	16

4. Calcium controlled transmitter release function

Depolarization of the IHC membrane leads to an increase in the calcium current, I_{Ca},

$$I_{\text{Ca}}(t) = G_{\text{Ca}}^{\max} m_{I_{\text{Ca}}}^3(t)(V(t) - E_{\text{Ca}}), \tag{A7}$$

where E_{Ca} is the reversal potential for calcium and $G_{\text{Ca}}^{\max}$ is the calcium conductance in the vicinity of the synapse, with all the channels open. $m_{I_{\text{Ca}}}(t)$ is the fraction of calcium channels that are open. Its steady state value, $m_{I_{\text{Ca}},\infty}$, is modeled by a Boltzmann function

$$m_{I_{\text{Ca}},\infty} = [1 + \beta_{\text{Ca}}^{-1} \exp(-\gamma_{\text{Ca}} V(t))]^{-1}, \tag{A8}$$

where β_{Ca} and γ_{Ca} are constants chosen to reflect published observations of calcium currents (see Table III), and $m_{I_{\text{Ca}}}(t)$ is a low-pass filtered function of $m_{I_{\text{Ca}},\infty}$

$$\tau_m \frac{dm_{I_{\text{Ca}}}(t)}{dt} + m_{I_{\text{Ca}}}(t) = m_{I_{\text{Ca}},\infty}, \tag{A9}$$

where τ_m is a calcium current time constant.

TABLE III. Parameters for control of presynaptic calcium levels. Source: Sumner *et al.* (2002, Table II).

		Calcium influx.	Calcium clearance
E_{Ca}, reversal potential (V)		0.066	0.066
β_{Ca}		400	400
γ_{Ca}		130	130
τ_m, calcium current time constant (s)		$1E-4$	$1E-4$
τ_{Ca}, calcium clearance time constant (s)			
	HSR	$1E-4$	$3.5E-4$
	MSR	$1E-4$	$1.5E-4$
	LSR	$1E-4$	$0.75E-4$
z, converts from $[Ca^{2+}]^3$ to probability		$2E33$	$2E42$
$G_{\text{Ca}}^{\max}$, maximum Ca^{2+} conductance			
	HSR	$7.2E-9$	$8E-9$
	MSR	$2E-9$	$8E-9$
	LSR	$1.6E-9$	$8E-9$
$[Ca^{2+}]_{\text{thr}}$, threshold			
	HSR	0	Not used
	MSR	$3.3E-14$	
	LSR	$1.4E-11$	

TABLE IV. IHC transmitter release parameters. Source: Meddis and O'Mard (2005).

y, replenishment rate (s^{-1})	3
l, loss rate (s^{-1})	2580
x, reprocessing rate (s^{-1})	30
r, recovery rate (s^{-1})	6580
M, maximum free transmitter quanta	10

Presynaptic calcium concentration $[Ca^{2+}](t)$ is modeled as a first-order low-pass filtered function of calcium current, $I_{\text{Ca}}(t)$. This has been changed slightly from the previous published formula to match units. This requires a change to $G_{\max}$ scalar but is otherwise equivalent.

$$\frac{d[Ca^{2+}](t)}{dt} = I_{\text{Ca}}(t) - [Ca^{2+}](t)/\tau_{[\text{Ca}]}, \tag{A10}$$

where τ_{Ca} is a time constant. The probability of the release of transmitter is proportional to the cube of $[Ca^{2+}]$ concentration

Original published model (calcium influx model):

$$k(t) = \max(([Ca^{2+}]^3(t) - [Ca^{2+}]_{\text{thr}}^3)z, 0), \tag{A11}$$

where $[Ca^{2+}]_{\text{thr}}$ is a threshold constant, z is a scalar for converting calcium levels into release rate.

In the calcium clearance model, the calcium threshold has been removed, leaving the the more transparent expression

$$k(t) = z\{[Ca^{2+}]^3(t)\}. \tag{A12}$$

See Table IV.

5. Quantal and probabilistic model of synaptic adaptation

More detailed accounts of transmitter release in a probabilistic form can be found in Hewitt and Meddis (1991) and Sumner (2002, 2003a, and 2003b). A description of the quantal version is found in Sumner (2002).

Individual vesicles of neurotransmitter (probably glutamate) are released from an *immediate presynaptic* store containing $q(t)$ transmitter vesicles into the synaptic cleft, $c(t)$, at a rate, $k(t)$, that is dependent on calcium concentration, $[Ca^{2+}](t)$. In the cleft, the transmitter disperses and some is lost from the system at a rate *l*. The remaining transmitter in the cleft is taken back into the cell into a reprocessing store containing $w(t)$ vesicles at a rate *r*. Here, it is repackaged into vesicles that are returned to the immediate store at a rate *x*. Additionally, $q(t)$ is continuously replenished with new transmitter vesicles at a rate $y[M-q(t)]$, where *M* represents the maximum number of transmitter quanta that can be held in the immediate store.

Neurotransmitter in the immediate store is quantal, and enters and leaves the immediate store stochastically. The stochastic transport of neurotransmitter is described by the function $N(n,\rho)$, in which each of *n* quanta has an equal probability of release, $\rho \cdot dt$, in a single simulation epoch. In the cleft and reprocessing stores, transmitter is a continuous quantity. This means, for instance, that the contents of the

TABLE V. MacGregor point neuron parameters Source: modified from Wiegrebe and Meddis (2004) to use international units.

Dendritic low-pass cutoff (Hz)	100
τ_m, membrane time constant (s)	$5E-4$
τ_{Gk}, potassium recovery time constant (s)	$4E-4$
b, increment in G_k (Siemens/s)	8000
$Th0$, resting threshold (V)	$16E-3$
E_k potassium reversal potential (V)	−10
R, membrane resistance (ohms)	$60E6$

reprocessing store must contain at least enough transmitter to make one vesicle before a quantum can rejoin the immediate store. The output from the synapse into the cleft is a stream of discrete events indicating vesicle releases, $N[q(t),k(t)]$.

The flow of transmitter between stores is simulated by the following equations:

$$\frac{dq(t)}{dt} = N(w(t),x) + N([M - q(t)],y) - N(q(t),k(t)), \tag{A13}$$

$$\frac{dc(t)}{dt} = N(q(t),k(t)) - lc(t) - rc(t), \tag{A14}$$

$$\frac{dw(t)}{dt} = rc(t) - N(w(t),x). \tag{A15}$$

Initial values for the variable quantities are found as follows (Meddis *et al.*, 1990):

$$c_0 = k_0 ym/[y(l+r) + k_0 l], \tag{A16}$$

$$q_0 = c_0(l+r)/k_0, \tag{A17}$$

$$w_0 = c_0 r/x. \tag{A18}$$

6. Auditory nerve response

An absolute refractory period lasting 0.75 ms was applied. Thereafter, a release event was converted into a spike on a probabilistic basis as a function of time since the last spike

$$P_{\text{conversion}} = 1 - \exp(t/0.0006). \tag{A19}$$

Each spike is counted and added to a peristimulus time histogram (PSTH) with a 0.0005-s bin width. When multiple fibers are used, all spikes are aggregated in the same PSTH. This then serves as the input to the next stage.

7. Sustained chopper model

The CN unit model is based on MacGregor's (1987) point neuron model. It consists of two stages: (1) input at the dendrites and (2) spike generation at the soma. The dendritic input stage applies a first-order low-pass filter to the AN PSTH to produce a representation of input current, $I(t)$, to the soma assuming a current input of 300 nA per spike when there are 20 fibers. If more fibers are used this value must be adjusted *pro rata*. See Table V.

The trans-membrane potential at the soma, E, is represented as a deviation from resting potential, E_r, and tracked using the equation

$$dE(t)/dt = -E(t)/\tau_m + I(t)\cdot R + Gk(t)\cdot[Ek - E(t)], \tag{A20}$$

where τ_m is the membrane time constant, R is the cell membrane resistance, E_k is the potassium reversal potential (relative to E_r), and $Gk(t)$ is the cell potassium conductance

$$dGk(t)/dt = -Gk(t)/\tau Gk + (b\cdot s), \tag{A21}$$

where τ_{Gk} is the potassium time constant, b is the increase in G_k following an action potential indicated when $s=1$. An action potential is initiated when the membrane potential exceeds a threshold $E(t) > Th0$. This threshold was fixed throughout. The original MacGregor neuron provides for the possibility that the $Th0$ can vary over time. This has been omitted here by setting his parameter c to 0.

[1]DSAM: Development software for Auditory Modeling, a library of compiled C-code routines for auditory modeling. AMS: auditory modeling system, an application for creating running and displaying complex auditory models using DSAM routines. This software is available from the authors. (http://www.essex.ac.uk/psychology/hearinglab/)

Clock, A. E., Salvi, R. J., Saunders, S. S., and Powers, N. L. (**1993**). "Neural correlates of temporal integration in the cochlear nucleus of the chinchilla," Hear. Res. **71**, 37–50.

Clock, A. E., Salvi, R. J., Wang, J., and Powers, N. L. (**1998**). "Threshold-duration functions of chinchilla auditory nerve fibers," Hear. Res. **119**, 135–141.

Eddins, D. A., and Green, D. M. (**1995**). "Temporal integration and temporal resolution," in *Hearing*, edited by B. C. J. Moore (Academic, San Diego), pp. 207–242.

Florentine, M., Fastl, H., and Buus, S. (**1988**). "Temporal integration in normal hearing, cochlear impairment, and impairment simulated by masking," J. Acoust. Soc. Am. **84**, 195–203.

Gerken, G. M. (**1979**). "Temporal summation of pulsate brain stimulation in normal and deafened cats," J. Acoust. Soc. Am. **66**, 728–734.

Gersuni, G. V. (**1965**). "Organization of afferent flow and the process of external signal discrimination," Neuropsychologia **3**, 95–109.

Heil, P., and Neubauer, H. (**2001**). "Temporal integration of sound pressure determines thresholds of auditory nerve fibers," J. Neurosci. **15**, 7404–7415.

Heil, P., and Neubauer, H. (**2003**). "A unifying basis of auditory thresholds based on temporal summation," Proc. Natl. Acad. Sci. U.S.A. **100**, 6151–6156.

Hewitt, M. J., and Meddis, R. (**1991**). "An evaluation of eight computer models of mammalian inner hair-cell function," J. Acoust. Soc. Am. **90**, 904–917.

Hewitt, M. J., and Meddis, R. (**1993**). "Regularity of cochlear nucleus stellate cells: A computational modeling study," J. Acoust. Soc. Am. **93**, 3390–3399.

Hewitt, M. J., and Meddis, R. (**1994**). "A Computer model of amplitude-modulation sensitivity of single units in the inferior colliculus," J. Acoust. Soc. Am. **95**, 2145–2159.

Holmes, S., Sumner, C., O'Mard, L. P., and Meddis, R. (**2004**). "The temporal representation of speech in a nonlinear model of the guinea pig cochlea," J. Acoust. Soc. Am. **116**, 3534–3545.

Krishna, B. S. (**2002**). "A unified mechanism for spontaneous-rate and first-spike timing in the auditory nerve," J. Comput. Neurosci. **13**, 71–91.

Levitt, H. (**1971**). "Transformed up and down methods in psychology," J. Acoust. Soc. Am. **49**, 467–477.

Liberman, M. C., and Kiang, N. Y. S. (**1978**). "Acoustic trauma in cats. Cochlear pathology and auditory-nerve activity," Acta Otolaryngol. Suppl. **358**, 1–63.

Lopez-Poveda, E. A., and Meddis, R. (**2001**). "A human nonlinear cochlear filterbank," J. Acoust. Soc. Am. **110**, 3107–3118.

MacGregor, R. J. (**1987**). *Neural and Brain Modeling* (Academic, San Diego).
Meddis, R., and O'Mard, L. P. (**2005**). "A computer model of the auditory nerve response to forward masking stimuli," J. Acoust. Soc. Am. **117**, 3787–3798.
Meddis, R., Hewitt, M. J., and Shackleton, T. (**1990**). "Implementation details of a computational model of the inner hair-cell/auditory-nerve synapse," J. Acoust. Soc. Am. **87**, 1813–1818.
Meddis, R., O'Mard, L. P., and Lopez-Poveda, E. A. (**2001**). "A computational algorithm for computing nonlinear auditory frequency selectivity," J. Acoust. Soc. Am. **109**, 2852–2861.
Sumner, C. J., Lopez-Poveda, E. A., O'Mard, L. P., and Meddis, R. (**2003a**). "Adaptation in a revised inner-hair cell model," J. Acoust. Soc. Am. **113**, 893–901.
Sumner, C. J., O'Mard, L. P., Lopez-Poveda, E. A., and Meddis, R. (**2003b**). "A nonlinear filter-bank model of the guinea-pig cochlea," J. Acoust. Soc. Am. **113**, 3264–3274.
Sumner, C. J., O'Mard, L. P., Lopez-Poveda, E. A., and Meddis, R. (**2002**). "A revised model of the inner-hair cell and auditory nerve complex," J. Acoust. Soc. Am. **111**, 2178–2189.
Viemeister, N. F., Shivapuja, G., and Recio, A. (**1992**). "Physiological correlates of temporal integration," in *Auditory Physiology and Perception*, edited by Y. Cazals, K. Horner, and L. Demany (Pergamon, Oxford), pp. 323–329.
Wiegrebe, L., and Meddis, R. (**2004**). "The representation of periodic sounds in simulated sustained chopper units of the ventral cochlear nucleus," J. Acoust. Soc. Am. **115**, 1207–1218.
Winter, I. M., Robertson, D., and Yates, G. K. (**1990**). "Diversity of characteristic frequency rate-intensity functions in guinea pig auditory nerve fibers," Hear. Res. **45**, 191–202.